Journal of Instrumentation

Boron-10 lined RPCs for sub-millimeter resolution thermal neutron detectors: Feasibility study in a thermal neutron beam

To cite this article: L.M.S. Margato *et al* 2019 *JINST* **14** P01017

Published by IOP Publishing for Sissa Medialab
Received: *September 25, 2018*
Revised: *December 11, 2018*
Accepted: *January 7, 2019*
Published: *January 17, 2019*

Boron-10 lined RPCs for sub-millimeter resolution thermal neutron detectors: Feasibility study in a thermal neutron beam

L.M.S. Margato,[a,1] **A. Morozov,**[a] **A. Blanco,**[a] **P. Fonte,**[a,b] **F.A.F. Fraga,**[c] **B. Guerard,**[d] **R. Hall-Wilton,**[e,f] **C. Höglund,**[e,g] **A. Mangiarotti,**[h] **L. Robinson,**[e] **S. Schmidt**[e,i] **and K. Zeitelhack**[j]

[a] *LIP-Coimbra, Departamento de Física, Universidade de Coimbra, Rua Larga, 3004-516 Coimbra, Portugal*
[b] *Coimbra Polytechnic - ISEC, Coimbra, Portugal*
[c] *Departamento de Física, Universidade de Coimbra, Rua Larga, 3004-516 Coimbra, Portugal*
[d] *ILL-Institut Laue-Langevin, 71 avenue des Martyrs - CS 20156 - FR-38042 GRENOBLE CEDEX 9, France*
[e] *European Spallation Source ERIC (ESS), P.O Box 176, SE-221 00 Lund, Sweden*
[f] *Mid-Sweden University, SE-85170 Sundsvall, Sweden*
[g] *Linköping University, IFM, Thin Film Physics Division, SE-581 83, Linköping, Sweden*
[h] *IFUSP, Institute of Physics, University of São Paulo, Brazil*
[i] *IHI Ionbond AG- Industriestraße 211, 4600 Olten, Switzerland*
[j] *Heinz Maier-Leibnitz Zentrum (MLZ), FRM-II, Technische Universität München, D-85748 Garching, Germany*

E-mail: margato@coimbra.lip.pt

Abstract: The results of an experimental feasibility study of a position sensitive thermal neutron detector based on a resistive plate chamber (RPC) are presented. The detector prototype features a thin-gap (0.35 mm) hybrid RPC with an aluminium cathode and a float glass anode. The cathode is lined with a 2 μm thick $^{10}B_4C$ neutron converter enriched in ^{10}B. A detection efficiency of 6.2% is measured at the neutron beam (λ = 2.5 Å) for normal incidence. A spatial resolution better than 0.5 mm FWHM is demonstrated.

Keywords: Neutron detectors (cold, thermal, fast neutrons); Resistive-plate chambers; Gaseous detectors

[1] Corresponding author.

https://doi.org/10.1088/1748-0221/14/01/P01017

2019 JINST 14 P01017

Contents

2019 JINST 14 P01017

1 Introduction

In the previous paper [1], we have introduced a new type of position sensitive neutron detector (PSND) based on thin-gap resistive plate chambers (RPC) and $^{10}B_4C$ neutron converters [2–4]. The results of simulations of Boron-10 lined RPCs with different designs, carried out with ANTS2 toolkit [5], have shown that RPC-based PSNDs have potential to reach high (>50%) detection efficiency for thermal neutrons in multilayer and inclined detector architectures [1]. This, along with fast timing (sub-ns time resolution [6, 7]) and high spatial resolution (< 100 µm [8, 9]) make the combination of RPCs with the state-of-the-art Boron-10 enriched solid neutron converters [2–4] an attractive detector technology for high precision PSNDs for applications in neutron scattering science (NSS), homeland security and geology. RPCs also offer several important practical advantages, such as insensitivity to magnetic field, intrinsic discharge-protection mechanism, high modularity and scalability, and low cost per unit area [10, 11].

Detection of neutrons with RPCs lined with solid converters was suggested already in 1991 by Calligarich et al., [12]. Those authors used as neutron converter a mixture of boron carbide powder with an epoxy resin to coat the RPC electrodes, made with phenolic resin (Bakelite). Two decades later, RPCs with solid converters were also developed for detection of back-scattered neutrons from hydrogen-rich explosive materials of antipersonnel land mines [13, 14]. However, the development of RPC-based PSNDs for NSS applications was not pursued and their application in high resolution and high detection efficiency detectors for thermal neutrons was not reported before.

This paper presents the results of an experimental feasibility study of a PSND prototype with a thin-gap hybrid RPC. The aluminium cathode of the RPC is lined with a 2 µm thick layer of $^{10}B_4C$. Deposition of the $^{10}B_4C$ converters, enriched in ^{10}B, has been performed at the Linköping University and in the ESS Detector Coatings Workshop and the prototype has been constructed at the LIP-Coimbra laboratory.

The prototype has been characterized on the CT2 monochromatic thermal neutron beam (λ = 2.5 Å) at the Institut Laue-Langevin (ILL). The results demonstrate that the hybrid RPC prototype is sensitive to thermal neutrons and exhibits a wide plateau with respect to the RPC polarization voltage. The detection efficiency is measured and compared with the results of the Monte Carlo simulations. Scans of the detector with a narrow neutron beam are performed and sub-millimeter spatial resolution of the detector is demonstrated.

2 Experimental setup

2.1 Hybrid RPC with $^{10}B_4C$ neutron converter

The feasibility of using ^{10}B-lined RPCs for PSNDs is evaluated in this study with a single-gap RPC prototype in the hybrid configuration [1]. Figure 1 shows a schematic drawing of the detector. The sensitivity to thermal neutrons originates from the neutron capture reaction ^{10}B(n,^{4}He)^{7}Li. The ^{7}Li and ^{4}He fission fragments can exit the converter into the gas-gap with sufficient energy to generate ionization followed by Townsend avalanches. A detailed description of the working principle of this detector can be found in the previous paper [1].

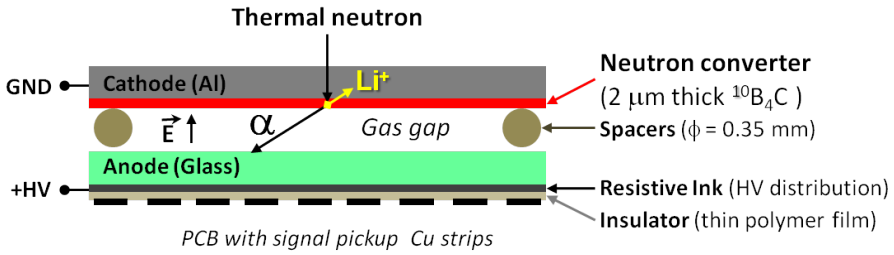

Figure 1. Schematic drawing of a single-gap hybrid RPC lined with a $^{10}B_4C$ neutron converter.

The aluminium cathode (1 mm thick, 8×8 cm^2 area) is lined with a 2 μm thick layer of $^{10}B_4C$ on the surface facing the gas-gap. The $^{10}B_4C$ coating with ^{10}B enrichment above 97% has been deposited onto one side of the aluminium plates at the Linköping University and in the ESS Detector Coatings Workshop in Linköping. The deposition has been performed at an industrial-scale DC magnetron sputtering system at a substrate temperature bellow 100°C to avoid deformation of the aluminium due to residual stresses in the coating. Further details on the deposition technique and parameters can be found in [2].

The float glass anode plate (0.35 mm thick, 8×8 cm^2) is lined on the surface opposite to the gas-gap with a thin layer of resistive ink. The function of this layer is to evenly distribute the high voltage (HV) over the entire electrode surface. Nylon monofilaments (0.35 mm diameter) are placed between the anode and the cathode plates (see figure 2) to define the gas-gap width.

The array of signal pick-up electrodes (2 mm wide copper strips with a pitch of 2.5 mm) is engraved on a 1.5 mm thick printed circuit board (PCB). The PCB is installed with the electrodes facing the anode resistive ink, insulated from it by a 50 μm thick acetate film (see figure 1).

2019 JINST 14 P01017

Figure 2. Photographs of the aluminium cathode plate lined with a 2 μm thick layer of $^{10}B_4C$ (a), and of the cathode lifted above the anode glass plate (b). The RPC electrodes are separated by 0.35 mm diameter nylon monofilaments (visible as the white lines on top of the anode) defining a gas-gap of uniform with.

2.2 Detector layout and setup at a neutron beam line

In order to evaluate the effect of the presence of the neutron converter on the hybrid RPC response, two RPCs have been assembled, identical in all aspects except that one of them (RPC-1) does not have a neutron converter, while the other one (RPC-2) has a 2 μm thick layer of $^{10}B_4C$ deposited on the cathode. Both RPCs are installed inside the same gas-tight chamber made from aluminium (Al alloy 5083), as shown in figure 3, to be tested in identical experimental conditions. The gas chamber is equipped with two 3 mm thick aluminium windows on opposite sides, each facing the cathode of the corresponding RPC. This arrangement allows to operate both RPCs in identical conditions with respect to the neutron beam irradiation by rotating the detector 180 degrees around the vertical axis.

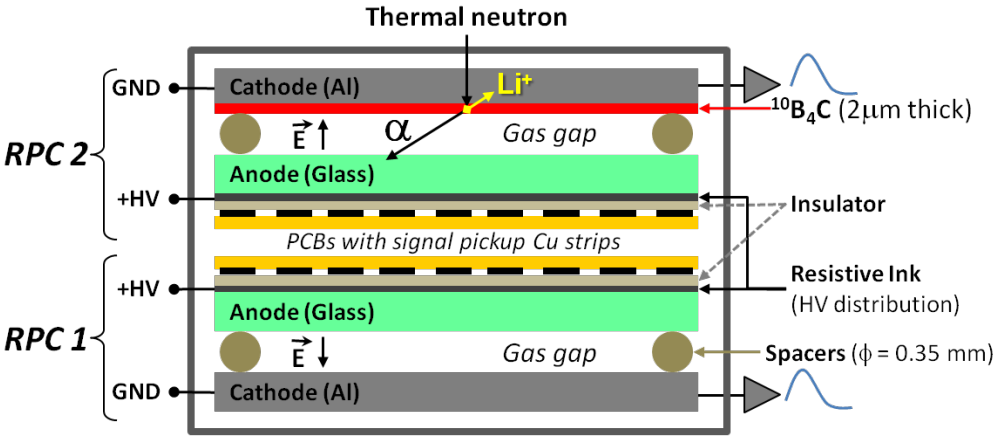

Figure 3. Schematic drawing of the detector gas chamber enclosing two single-gap hybrid RPCs: RPC-1 does not have a neutron converter, while the cathode of RPC-2 is lined with a 2 μm thick layer of $^{10}B_4C$.

The gas chamber is filled with tetrafluoroethane ($C_2H_2F_4$) at atmospheric pressure. The gas, supplied by Linde, has industrial purity grade. All experiments in this study are performed with the gas flow rate of ≈ 2 cc/min and the ambient temperature of 25°C.

2019 JINST 14 P01017

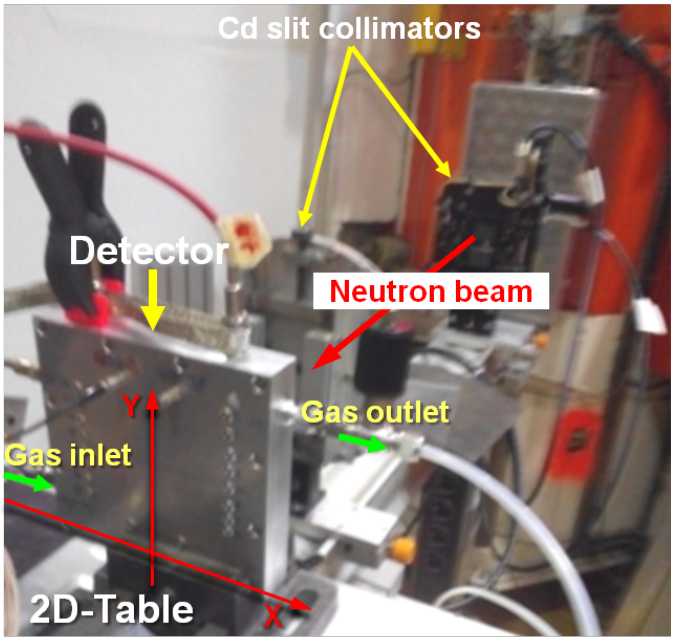

Figure 4. Detector installed on a 2D moving stage on the CT2 neutron beam line (λ = 2.5 Å) at ILL. The beam is collimated by a pair of orthogonal cadmium slits (vertical and horizontal directions) mounted on an optical bench.

The gas inlet and outlet valves are mounted on opposite corners of the gas chamber (see figure 4) in order to improve gas renewal. All parts of the gas system are interconnected with polytetrafluoroethylene (PTFE) tubes.

A polarization potential up to 2.8 kV is applied to the anodes using a CAEN N471A power supply. The total current is monitored using the internal gauge of the module (1 nA resolution).

The setup has been installed on the CT2 monochromatic thermal neutron beam line (λ = 2.5 Å) at ILL (see figure 4). The gas chamber is positioned on a 2D moving stage and two mutually-perpendicular cadmium slits of adjustable width are used to define the irradiated area. The beam is always incident orthogonally to the entrance window.

After installation at the beam line, the gas chamber has been flushed with the working gas at a flow rate of about 10 cc/min for 4 hours. Before starting measurements, the RPCs have been kept polarized at 2.8 kV for 12 hours. After this procedure the dark current is below 1 nA.

2.3 Electronic readout and DAQ system

For the neutron sensitivity measurements, the signals induced on the RPC cathode plate, kept at the ground potential, are readout by a charge sensitive preamplifier (sensitivity of 1 V/pC) and then fed into a linear amplifier (Canberra 2021) with the shaping time of 1 μs. The output of the amplifier is connected to a single-channel analyzer (SCA, ORTEC model 553). Finally, the digital output of the SCA is read by a counter module. The lower level threshold of the SCA is set to the level corresponding to 0.1 pC at the input of the preamplifier, in order to suppress electronic noise. The calibration of the entire signal processing chain has been performed using an ORTEC 448 pulser and a 2 pF calibrated capacitor to inject a known charge in the input of the preamplifier.

2019 JINST 14 P01017

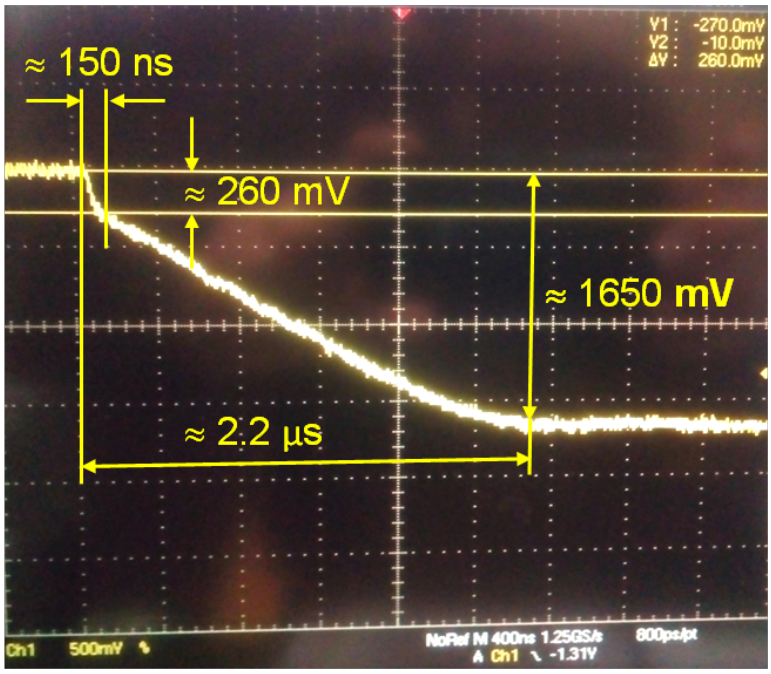

Figure 5. Cathode pulse at the output of the inverting charge preamplifier shown at the screen of a Tektronix TDS7104 oscilloscope (the amplitude and time scales are 500 mV/div and 400 ns/div, respectively). At the beginning of the pulse there is a fast electronic component followed by a slow ionic one. Integration during the first 150 ns results in the collection of ≈ 15% of the total induced charge.

The signal pick-up strips, providing the neutron event position information, are readout with a custom data acquisition system based on the MAROC chip [15]. MAROC3 features 64 inputs, each equipped with a low impedance preamplifier with adjustable gain and a slow shaper with a configurable time constant. The charge is digitized by the on-chip Wilkinson ADC (12 bits). The slow shaper is set to the maximum possible integration time (time constant of ~ 150 ns), resulting in the collection of ≈ 15% of the total charge induced in the RPC pick-up electrodes during a neutron event (see figure 5).

For practical reasons, only 16 signal pick-up strips in the central area of the PCB are connected to the acquisition system. The remaining strips, 8 on the left and 8 on the right side, are grounded. The digitized signals are transferred to a PC via a USB connection and stored for further processing. After removing pedestals, the signals from the three adjacent strips with the highest collected charge are used to calculate the position of the neutron capture by applying the center of gravity (CoG) algorithm [16].

3 Results and discussion

3.1 Plateau measurement

The sensitivity to thermal neutrons has been measured for both RPCs (RPC-1 without and RPC-2 with the neutron converter, see section 2.2) as a function of the polarization voltage using a monochromatic (λ = 2.5 Å) neutron beam.

2019 JINST 14 P01017

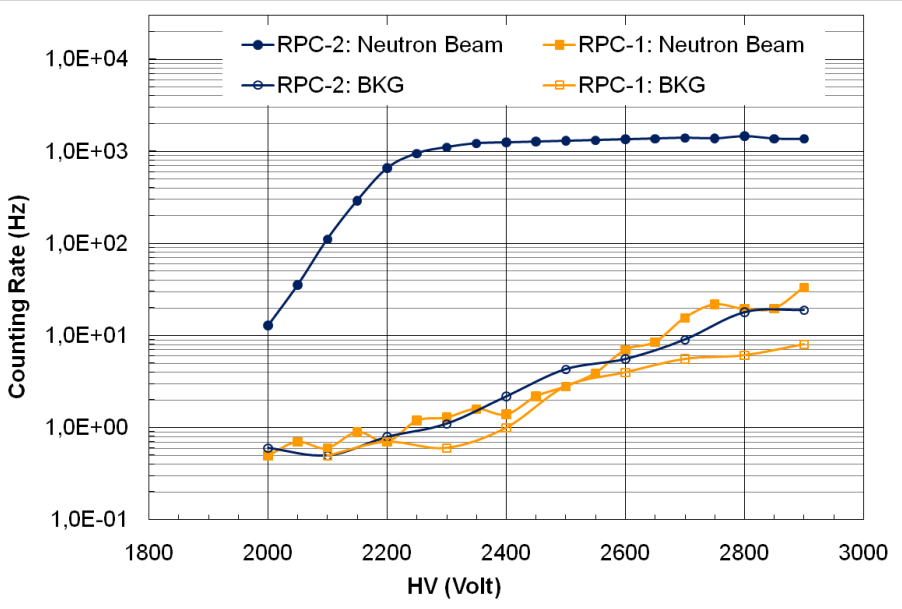

Figure 6. Counting rate recorded with RPC-1 and RPC-2 as a function of the polarization voltage with and without neutron beam irradiation. The square and circular markers designate the results for RPC-1 and RPC-2, respectively. In both cases the markers are filled when the beam is on and are empty when the beam is off.

Figure 6 shows the counting rate as a function of the polarization voltage with and without neutron beam irradiation. The beam is attenuated by 9 mm of acrylic glass to avoid saturation (see section 3.2). The irradiated area on the detector is $2 \times 4\,\mathrm{cm}^2$, which corresponds to the largest possible neutron beam cross-section area available with this setup. Since the signals are read on the metallic cathode, the background count rate had the contribution of the entire active area of the RPC ($8 \times 8\,\mathrm{cm}^2$).

The counting rate of RPC-2 recorded with the beam exhibits a strong increase with polarization potential until $\approx 2.3\,\mathrm{kV}$ and then stabilizes showing a wide plateau well above the counting rate recorded without beam. On the other hand, the counting rates of RPC-1 recorded with and without beam are very similar, confirming insensitivity of the RPC without the neutron converter to thermal neutrons. This difference in the response to the beam demonstrates the feasibility of using hybrid ^{10}B-RPCs for thermal neutron detection.

The fact that the counting rate of RPC-1 with and without the beam is essentially the same (considering the uncertainties) for polarization voltages up to 2.5 kV (see figure 6) also suggests that the prototype has low sensitivity to the gamma rays produced by nuclear interactions of neutrons with the materials of the detector and the experimental setup, most importantly the cadmium slits. For potentials above 2.5 kV the counting rate recorded with beam is higher than the one without beam, and the difference increases with potential, which can be explained by an increase in the sensitivity of the RPC to the gamma rays generated due to the neutron beam irradiation. Note that the neutron sensitivity plateau is reached with RPC-2 at a significantly lower potential ($\approx 2.3\,\mathrm{kV}$).

A background counting rate of less than $2 \times 10^{-2}\,\mathrm{Hz/cm}^2$ is measured for both RPCs operated with a voltage of 2.4 kV. For the voltages above 2.5 kV, the difference in the background level

2019 JINST 14 P01017

of RPC-1 and RPC-2 (figure 6) is most likely explained by imperfections of the RPC electrode surfaces [17, 18].

The RPC counts recorded without beam originate from two main processes. The first one is spontaneous generation of avalanches in the gas-gap appearing, for example, in the vicinity of micro-defects at the electrodes surface. The second one is energy deposition due to the radiation background, which includes cosmic rays, fast neutrons leaking from the reactor and fission fragments from the decay of radioactive impurities present in the materials of the RPC electrodes. The background counting rate of the RPCs can be reduced using several approaches. One of them is to improve the surface quality [18] of the glass and aluminium plates. Another one is to optimize the working gas mixture minimizing the number of streamers [19–21]. Also, several strategies for reducing the background connected to the presence of traces of radioactive isotopes in aluminium alloys [22] were suggested [23] for ^{10}B based thermal neutron detectors. These strategies include use of radiopure materials or, alternatively, introduction of a thin layer of nickel at the surface of aluminium plates in order to stop alpha particles produced in the decay chains of radioactive impurities, such as, e.g., thorium and uranium.

3.2 Detection efficiency

The counting rate of RPC-2 has been recorded as a function of the neutron beam flux in order to establish the range where the detector is operating in linear mode. The flux was adjusted by changing the number of acrylic glass attenuators placed in front of the first cadmium slit (see section 2.2). The RPC is operated at 2.4 kV, which is well within the plateau (see figure 6).

The results are shown in figure 7 for two areas (1 and 8 cm^2) irradiated with the beam. For comparison, the figure also gives the counting rate recorded with a ^{3}He-tube (90% efficiency at 2.5 Å) for 1 cm^2 beam area. The choice of 1 cm^2 area is made to avoid loss of detection efficiency by ^{3}He-tube, due to its geometry (the tube diameter is 5 cm), while 8 cm^2 is the maximum beam area available at the beam line. Note that the counting rate of RPC-2 scales linearly with the irradiated area (factor of ≈ 8).

Figure 7 demonstrates that the counting rate measured with RPC-2 remains linear up to $\approx$ 1 kHz/cm^2. Above this value, RPC-2 starts losing efficiency, which is expected taking into account that the resistive anode is made from common float glass, which has quite high resistivity ($\sim 10^{12}\,\Omega \cdot$ cm). Similar counting rates (from 1 to 3 kHz/cm^2) were already reported for float glass RPCs designed to detect minimum ionizing particles (MIPs) [24, 25].

The detection efficiency is calculated as the ratio of the number of detected neutron events per second, corrected for the background, to the neutron beam flux incident on the sensitive area of the detector. The flux was measured with the ^{3}He tube. The background counting rate was recorded in the same conditions but in the absence of beam. For the irradiated area of 1 cm^2 and the combined attenuator thickness of 9 mm, the neutron detection efficiency of RPC-2 is (6.2 ± 0.6)%.

This calculated efficiency value practically matches the value of 6.1% obtained for 2.5 Å neutrons in simulations of the detector with the ANTS2 toolkit [5] (see [1] for the description of the simulation procedure).

As expected, the detection efficiency of the RPC with a single converter layer orientated orthogonally to the neutron beam is quite low. However, as described in [1], ^{10}B hybrid RPC

2019 JINST 14 P01017

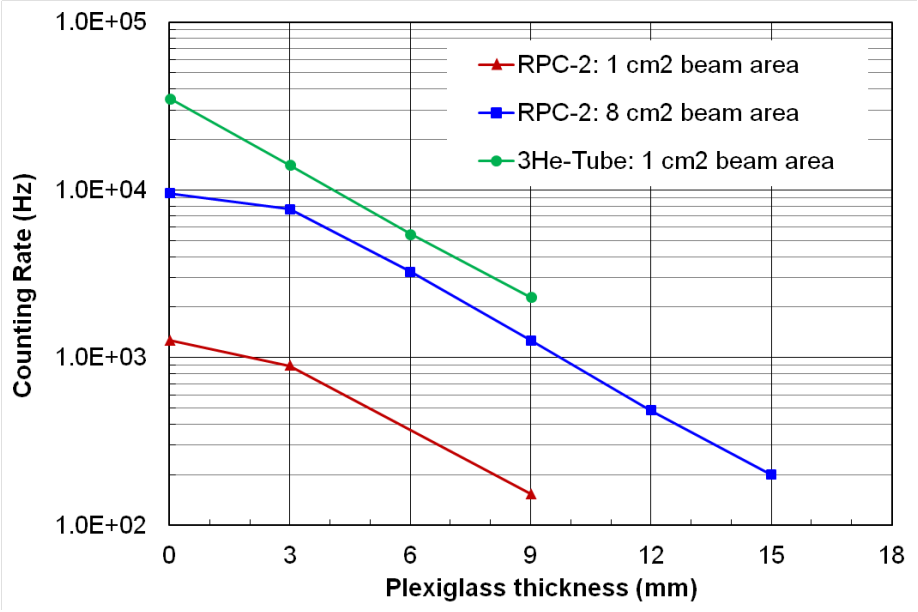

Figure 7. Counting rate, measured with RPC-2 and the ^{3}He tube, as a function of the combined thickness of the acrylic glass attenuators. The RPC-2 data are shown for two irradiated areas (1 and 8 cm^2); the data for the ^{3}He tube were recorded with the area of 1 cm^2.

PSNDs with significantly higher efficiencies can be designed using a multilayer configuration or orienting the RPC at a small angle with respect to the neutron beam.

3.3 Spatial resolution

For evaluation of the spatial resolution of the detector prototype, the collimators are adjusted to define a narrow beam of 0.5 mm by 40 mm (X and Y directions, respectively). The RPC polarization potential is set to 2.6 kV (cathode grounded) and the neutron beam is attenuated by 6 mm of acrylic glass, assuring operation of the detector in the liner regime (see section 2.2).

The X positions of the neutron capture events are calculated with the center of gravity algorithm using the three neighboring strips with the highest signal amplitude. The results of the reconstruction procedure for three positions of the detector (step of 0.5 mm in X direction) are presented in figure 8.

The distributions of the reconstructed positions shown in figure 8 suggest that the spatial resolution is $\leq$ 0.5 mm (FWHM). Note that the intrinsic resolution of the detector should be better taking into account that the beam width is 0.5 mm.

The profile of the distribution of the reconstructed positions (figure 8) is different from the shape one might expect: a uniform distribution (0.5 mm FWHM) convoluted with a narrow bell-shaped curve. The observed distribution appears mainly due to distortions introduced by the centroid reconstruction algorithm, which assumes linear dependence of the induced signal in a pick-up electrode with the distance to the event position. In contrast to this assumption, the strip response function (SRF), describing this dependence, can have a complex profile and strongly depends on the spread of the signals by the layer of resistive ink [26] as well as on the RPC geometry. A significant improvement in the fidelity of the reconstruction is expected to be achieved by applying a correction function to the results of the centroid reconstruction [27] or by using a more

2019 JINST 14 P01017

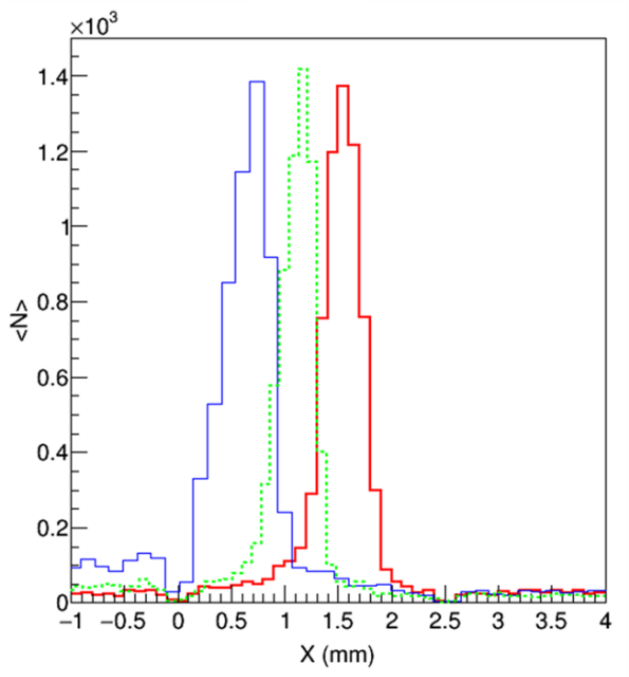

Figure 8. Distribution of the reconstructed X positions of the neutron events recorded with RPC-2 at three different positions (0.5 mm step in X direction). The neutron beam width is 0.5 mm and the pick-up electrode pitch is 2.5 mm.

sophisticated reconstruction method, such as, e.g., statistical reconstruction [28]. Both approaches require calibration data recorded by scanning the detector with a narrow neutron beam using a small step. Another factor which can affect the distribution profile is neutron scattering on the collimators, on the entrance window and inside the detector.

Note that the offset of the centroid of the induced charge from the true neutron capture position should be very small for this type of detector due to the narrow gas-gap (0.35 mm) and the anti-parallax effect of the electron avalanche development in RPCs described in [1].

4 Conclusions

This study demonstrates the feasibility of using thin-gap hybrid RPCs with $^{10}B_4C$ neutron converters for position sensitive thermal neutrons detectors. For the detector prototype with a single converter layer a detection efficiency of 6.2% is measured with a monochromatic neutron beam (λ = 2.5 Å) at normal incidence, which agrees well with the results of the Monte Carlo simulations (6.1% [1]).

A sub-millimetre spatial resolution ($\leq$ 0.5 mm FWHM) is demonstrated. The results suggest that the intrinsic resolution of the detector should be even better, since the contribution from the 0.5 mm wide collimator has not been deconvoluted from that value.

The fast timing of RPCs [6] should allow to measure the neutron time-of-flight (TOF) with nanosecond time resolution, which makes this type of detector also well suited for energy-selective or fast dynamic neutron imaging. The anode material of the prototype tested in this study was common float glass with high resistivity ($\sim 10^{12}\,\Omega \cdot$ cm), which limits the maximum counting rate

2019 JINST 14 P01017

of the detector ($\leq$ 1 kHz/cm^2). It should be possible to improve this value using lower resistivity anode materials and lower polarization voltages [29–31].

As discussed in [1], RPCs based PSNDs in multilayer and inclined geometries should be able to operate at high counting rates (the counting rate scales nearly linearly with the number of layers and with inverse sine of the angle of incidence) and provide detection efficiency exceeding 50%. Currently we are working on the characterization of the next generation prototype featuring $^{10}B_4C$ lined double-gap RPCs in a multilayer architecture.

Acknowledgments

This work was supported in part by the European Union's Horizon 2020 research and innovation programme under grant agreement No 654000. Richard Hall-Wilton, Carina Höglund, Linda Robinson, and Susann Schmidt would like to acknowledge the financial support of the EU H2020 Brightness Project, grant agreement 676548.

References

[1] L.M.S. Margato and A. Morozov, *Boron-10 lined RPCs for sub-millimeter resolution thermal neutron detectors: Conceptual design and performance considerations*, 2018 *JINST* **13** P08007 [arXiv:1806.07167].

[2] C. Höglund et al., *B_4C thin films for neutron detection*, *J. Appl. Phys.* **111** (2012) 104908.

[3] S. Schmidt, C. Höglund, J. Jensen, L. Hultman, J. Birch and R. Hall-Wilton, *Low-temperature growth of boron carbide coatings by direct current magnetron sputtering and high-power impulse magnetron sputtering*, *J. Mater. Sci.* **51** (2016) 10418.

[4] C. Höglund, K. Zeitelhack, P. Kudejova, J. Jensen, G. Greczynski, J. Lu et al., *Stability of $^{10}B_4C$ thin films under neutron radiation*, *Radiat. Phys. Chem.* **113** (2015) 14.

[5] ANTS2 webpage, http://coimbra.lip.pt/ants/ants2.html.

[6] A. Blanco et al., *In-beam measurements of the HADES-TOF RPC wall*, *Nucl. Instrum. Meth.* **A 602** (2009) 691.

[7] A.N. Akindinov et al., *Latest results on the performance of the multigap resistive plate chamber used for the ALICE TOF*, *Nucl. Instrum. Meth.* **A 533** (2004) 74.

[8] C. Iacobaeus, P. Fonte, T. Francke, J. Ostling, V. Peskov, J. Rantanen et al., *The Development and Study of High-Position Resolution (50 micron) RPCs for Imaging X-rays and UV photons*, *Nucl. Instrum. Meth.* **A 513** (2003) 244 [physics/0210006].

[9] A. Blanco, P. Fonte, L. Lopes, P. Martins, J. Michel, M. Palka et al., *TOFtracker: Gaseous detector with bidimensional tracking and time-of-flight capabilities*, 2012 *JINST* **7** P11012.

[10] R. Santonico and R. Cardarelli, *Development of Resistive Plate Counters*, *Nucl. Instrum. Meth.* **187** (1981) 377.

[11] R. Cardarelli, A. Di Ciaccio and R. Santonico, *Performance of a resistive plate chamber operating with pure CF_3Br*, *Nucl. Instrum. Meth.* **A 333** (1993) 399.

[12] E. Calligarich et al., *The resistive plate counter as a neutron detector*, *Nucl. Instrum. Meth.* **A 307** (1991) 142.

2019 JINST 14 P01017

[13] M. Abbrescia, T. Mongelli, V. Paticchio, A. Ranieri and R. Trentadue, *Resistive plate chambers as thermal neutron detectors*, *Nucl. Phys. Proc. Suppl.* **125** (2003) 43.

[14] R. Arnaldi et al., *Resistive plate chamber for thermal neutron detection*, *Nucl. Instrum. Meth.* **B 213** (2004) 284.

[15] S. Blin, P. Barrillon and C. de La Taille, *MAROC, a generic photomultiplier readout chip*, 2010 *JINST* **5** C12007.

[16] G. Charpak, G. Melchart, G. Petersen and F. Sauli, *High Accuracy Localization of Minimum Ionizing Particles Using the Cathode Induced Charge Center of Gravity Readout*, *Nucl. Instrum. Meth.* **167** (1979) 455.

[17] C. Lu, *RPC electrode material study*, *Nucl. Instrum. Meth.* **A 602** (2009) 761.

[18] RD51 collaboration, *Research on discharges in micropattern and small gap gaseous detectors*, arXiv:0911.0463.

[19] P. Camarri, R. Cardarelli, A. Di Ciaccio and R. Santonico, *Streamer suppression with SF-6 in RPCs operated in avalanche mode*, *Nucl. Instrum. Meth.* **A 414** (1998) 317.

[20] V. Koreshev, V. Ammosov, A.A. Ivanilov, Yu. Sviridov, V. Zaets and A. Semak, *Operation of narrow gap RPC with tetrafluoroethane-based mixtures*, *Nucl. Instrum. Meth.* **A 456** (2000) 46.

[21] M. Abbrescia, V. Cassano, S. Nuzzo, G. Piscitelli, D. Vadruccio and S. Zaza, *New gas mixtures for resistive plate chambers operated in avalanche mode*, *Nucl. Instrum. Meth.* **A 661** (2012) S190.

[22] M. Leroy, *Alpha Rays Emitting Impurities in Ultra Pure Aluminum Evolution Through the Successive Refining Steps*, *J. Phys. IV France* **5** (1995) C7-99.

[23] J. Birch, J.-C. Buffet, J.-F. Clergeau, J. Correa, P. van Esch, M. Ferraton et al., *In-beam test of the boron-10 multi-grid neutron detector at the IN6 time-of-flight spectrometer at the ILL*, *J. Phys. Conf. Ser.* **528** (2014) 012040.

[24] A. Akindinov et al., *A study of the multigap RPC at the gamma irradiation facility at CERN*, *Nucl. Instrum. Meth.* **A 490** (2002) 58.

[25] W. Zhu et al., *A thin float glass MRPC for the outer region of CBM-TOF wall*, *Nucl. Instrum. Meth.* **A 735** (2014) 277.

[26] G. Battistoni, P. Campana, V. Chiarella, U. Denni, E. Iarocci and G. Nicoletti, *Resistive cathode transparency*, *Nucl. Instrum. Meth.* **202** (1982) 459.

[27] M.S. Dixit, J. Dubeau, J.P. Martin and K. Sachs, *Position sensing from charge dispersion in micropattern gas detectors with a resistive anode*, *Nucl. Instrum. Meth.* **A 518** (2004) 721 [physics/0307152].

[28] H.H. Barrett, W.C.J. Hunter, B.W. Miller, S.K. Moore, Y. Chen and L.R. Furenlid, *Maximum-likelihood methods for processing signals from gamma-ray detectors*, *IEEE Trans. Nucl. Sci.* **56** (2009) 725.

[29] J.-B. Wang et al., *Development of multi-gap resistive plate chambers with low-resistive silicate glass electrodes for operation at high particle fluxes and large transported charges*, *Nucl. Instrum. Meth.* **A 621** (2010) 151.

[30] A. Laso Garcia, R. Kotte, L. Naumann, D. Stach, C. Wendisch, J. Wüstenfeld et al., *High-rate timing resistive plate chambers with ceramic electrodes*, *Nucl. Instrum. Meth.* **A 818** (2016) 45.

[31] A. Akindinov et al., *Radiation hard ceramic RPC development*, *J. Phys. Conf. Ser.* **798** (2017) 012136.

2019 JINST 14 P01017